JOURNAL OF THERMOPHYSICS AND HEAT TRANSFER
Vol. 23, No. 1, January–March 2009

Numerical and Experimental Investigation of the Origin of a Rarefied Jet

G. Gaffuri*
Polytechnic University of Marche, I-60131 Ancona, Italy
and
L. Marino†
University of Rome "La Sapienza," I-00184 Roma, Italy

DOI: 10.2514/1.36237

We investigate the flow region close to a cylindrical nozzle from which a free rarefied jet is issuing. Analytical, numerical, and experimental procedures are used to completely describe the aerodynamic flowfield from the upstream stagnation chamber, through the nozzle, and, finally, to the downstream ambient region. The combined theoretical–experimental investigation addresses the shortage of results in the literature concerning rarefied flow through finite length tubes, particularly in the region close to the jet origin. We also investigate the sensitivity of the jet characteristics to the velocity profile at the nozzle exit. Attention is paid to the physical differences between a continuum flow and a rarefied gas flow operating in the same geometrical conditions. The analytical expressions are derived from free molecular kinetics, the computational code is based on the direct simulation Monte Carlo method, and the experimental investigation uses measurements from a Patterson impact pressure probe. The broader implications of the results are discussed.

Nomenclature

D	=	internal diameter of the nozzle
d	=	molecule diameter
H	=	height of the slot of the probe
Kn	=	Knudsen number
k	=	Boltzmann constant
L	=	nondimensional height of the slot of the probe
$\dot{m}$	=	mass flow rate
N	=	number of computational cells
N_p	=	number of representative molecules
n	=	molecule number density
P	=	mean pressure
p	=	local pressure
R	=	radius of the computational domain
$\mathcal{R}$	=	constant of the gas
S	=	molecular speed ratio
s	=	nondimensional width of the slot of the probe
T	=	temperature
u	=	macroscopic velocity along the X axis
X, Y, Z	=	orthogonal coordinates
W	=	width of the slot of the probe
α	=	angular position of the sounding tube
γ	=	ratio of the specific heat
ΔL	=	length of the computational domain
Δt	=	time step
λ	=	mean free path of the gas
$\langle\ \rangle$	=	mean value over the nozzle area

Subscripts

amb	=	ambient condition
e	=	nozzle exit
i	=	nozzle inlet
m	=	mean value over the slot area of the probe
0	=	stagnation condition

Superscript

$*$	=	dimensional quantities

Received 17 December 2007; revision received 30 July 2008; accepted for publication 5 August 2008.

*Department of Energetics, Via Brecce Bianche.
†Department of Mechanics Aeronautics, Via Eudossiana 18.

I. Introduction

THE free gaseous jet is a model problem in fluid dynamics and can be used to test analytical solutions and computational simulations due to its relatively simple geometrical configuration. Apart from being of academic interest, free jets are important to a large number of scientific and technical applications. Jets operating in a rarefied gas find application in micro- and nanodevices, as well as in more conventional devices such as space thrusters, calibration nozzles, miniature diffusion devices, and vacuum apparatuses.

There is a vast amount of literature concerning the physics of jets, yet open questions still remain. To the authors' knowledge, the first experimental results showing the velocity distribution along the axis of a short jet nozzle for flows from the rarefied to continuum regime have only been recently presented by Koppenwallner et al. [1]. The mathematical modelling and experimental data collection needed to study rarefied jets are difficult due to the characteristics of the region close to the jet origin, where initial conditions must be obtained for any further calculation of the jet behavior. At the jet origin, there is equal influence from both the upstream "history" of the fluid and from the downstream ambient region. The study of the jet cannot be properly made without an evaluation of the flow development from the initial to the final state through the nozzle. This influence has been fully investigated for continuum incompressible and compressible flows, but due to the difficulties of rarefied jets, many of their aspects have been only partially investigated. In particular, the region very close to the nozzle exit and at the origin of the jet has not been fully studied.

The present work is devoted to a complete study of a rarefied jet, from its generation, through the nozzle, and, finally, to its expansion as a free molecular stream. Particular attention is paid to the initial region. The main contributions of this work are the full numerical evaluation of the jet characteristics ranging from the transitional to the free molecular regime, an investigation of the sensitivity of the jet development to the initial issuing conditions, a combined numerical–analytical calculation procedure for a jet of free molecules, an

experimental validation of the numerical analysis, and a guideline for calibrating complex experimental facilities as compared with very accurate numerical simulations.

Our review of related scientific literature will be limited to a discussion of rarefied jets and plumes. A good general presentation of the subject is an article by Rebrov [2], and more papers that include experiments and simulations for partial aspects of the subject can be found in [3–14].

Of these works, the only full numerical investigation of the aerodynamics for a limit situation of a rarefied jet was carried out by Sharipov [13] for the flow across an orifice. Another recent experimental and computational work investigated the characteristics of the rarefied flow through short tubes [4]. This work, by Lilly et al. [4], relates to the present work as both use the direct simulation Monte Carlo (DSMC) method for the numerical investigation. Also, Lilly et al. describe the importance and relevance of rarefied flows for microdevices. However, this previous work dealt with a jet nozzle at Knudsen numbers mostly smaller than what we used in our experiments and computations.

Our numerical approach and corresponding simulations were based on the DSMC method, which is known to provide accurate descriptions of rarefied gas flow situations [4,11,13]. We adopted the DSMC procedure from a numerical code that was previously used by the authors with excellent results [15,16]. With this code, we considered the jet problem in detail from the initial formation in the upstream stagnation chamber to the jet flow at the nozzle inlet.

The accuracy of the DSMC method has been analytically and, more importantly, experimentally scrutinized since Bird's introduction in the late 1960s [17]. Therefore, the DSMC method should attain a fairly high degree of predictive accuracy when a free molecular jet situation is dealt with. However, the results that will be presented show that the DSMC method needs a long computational time and well-imposed boundary conditions as one considers complex geometries. Even though the Knudsen number in the downstream falls in the free molecular regime, enough collisions are still present to influence the aerodynamic field. A problem similar to the one discussed here is numerically solved by Cai and Boyd [18] for the jet far field, and their computational code imposes the absence of molecular collisions, in so simplifying the free molecular flow simulation. A detailed description of the entire flow domain is needed due to the sensitivity of the jet characteristics to its initial conditions.

Our obtained results that will presented here are validated by comparing the numerical data with the experimental data. Furthermore, because the jet at the nozzle exit is in a free molecular condition, we developed a procedure to combine the numerical DSMC solution with an analytic free molecular expression, applying from the nozzle exit to the downstream ambient region. Finally, the sensitivity to the initial conditions was studied by analytical relationships for the case of a free molecular flow.

The experimental portion of this work occurred in highly rarefied conditions and was time consuming to perform. The experimental times increase as the size of the pressure sounding probe decreases. Conversely, a larger probe size requires a larger test area and, correspondingly, a more expensive rig and experiment. A Patterson impact pressure probe was adopted in our experiments, allowing us to decrease the operation time and to work on a small domain so that our apparatus costs were reduced.

Patterson probes have been extensively adopted in both the continuum regime and with free molecular flow [19] for cases in which the transverse dimensions of the jet are sufficiently large compared with the width of the measuring slot of the probe. Rosenhauer et al. [20] previously investigated a jet issuing from a supersonic nozzle and compared their results with those from a hybrid Navier–Stokes/DSMC procedure. However, in their work the fluid is continuous through the nozzle, and the Reynolds and Mach numbers at the nozzle exit also corresponded to a continuous fluid. The Patterson probe is reasonably fast to operate; however, one of its limitations is the relative dimension of its slot compared with the jet domain. Therefore, we numerically evaluated the gas state at the nozzle exit and validated our numerical code using the mean pressure distribution measured by the probe. To summarize, the objective of our work is a complete study, both experimental and theoretical, of the generation and development of a rarefied jet. The analysis of the thermofluid dynamic field is performed over the entire domain (stagnation chamber, nozzle, and test chamber), with particular attention to the flow in the nozzle and near the exit region. The experiments are run to validate the numerical values. The main parameters that influence the flow are investigated, and the sensitivity of the numerical solution to the boundary conditions is evaluated.

The flow physics of a rarefied jet presents several peculiarities compared with a jet in the continuum regime. In particular, if the gas begins its expansion through the nozzle in density conditions corresponding to a transitional flow, then that expansion will cause the gas molecules to reach density values that are close to the free molecular regime. Subsequently, the stream in the test chamber is absent of the phenomena typical of compressible continuum jets (e.g., shock waves, Mach disk), and the free molecules close to the jet origin move rapidly along straight trajectories.

In the compressible continuum, expansion of the fluid is associated with an increase in velocity and a decrease in density and pressure. In a free molecular flow, the jet of molecules expands from the nozzle exit with an associated decrease in density and pressure; however, the velocity of each molecule, in the absence of collisions, remains constant along the trajectory. Faster particles reach a fixed location in less time than slow particles. Hence, from a location far from the exit, a higher number of faster particles will be observed, and the macroscopic average speed will increase (see the exact analytical solution and DSMC simulation results by Cai and Boyd [18]).

Because the physical ambient region cannot be totally empty, small variations of velocity are still possible due to collisions with other molecules or with the walls. Other phenomena typical of a continuum regime, such as complex compression and expansion wave systems, are absent. Furthermore, the flow has negligible sensitivity to the pressure distribution at the jet origin, as is expected for a flow without collisions; yet, there is a noticeable sensitivity to the velocity conditions at the nozzle exit.

In light of these phenomena associated with rarefied jets, it can be understood why the numerical results, although highly reliable, should be compared with and validated by the experimental investigation. The DSMC method provides perhaps the closest representation of the actual physics in spite of, or just because of, its simple approach, which is supported by a great deal of experience.

In the following sections, we provide a short description of the experimental apparatus and a brief account of the adopted probe. Next, we describe the mathematical methods and report on the results of the calculations and experiments. Finally, we show the results and discuss the sensitivity of the jet characteristics to the velocity profile at the nozzle exit.

II. Experimental Rig

The early experiments were carried out at the Department of Energetics at the Polytechnic University of Marche in Ancona, Italy. Subsequent experiments were conducted at the Aerodynamics Laboratory of the Department of Mechanics and Aeronautics at the University "La Sapienza" in Rome. The experimental rig is shown in Fig. 1. Nitrogen flows from a high-pressure bottle to a stagnation chamber through a reduction valve, a gas flow meter, and a controller. The chamber is connected to a large test section via a cylindrical inlet nozzle, through which the gas expands into the test region. The length of the nozzle is 9 mm and its internal diameter, D, is 6 mm. The downstream wall of the test section contains an exit valve that corresponds to the inlet of a system of vacuum pumps. The low pressure is obtained by a Pfeiffer turbomolecular pump, and the limit vacuum in the system is about 10^{-6} Pa. A Patterson probe is mounted inside the test section on a support; the support can move in the axial and transversal directions of the cylindrical chamber and can rotate a few degrees around an axis normal to the jet axis.

Temperature and pressure measurements in the chambers are provided by absolute manometers, by the heads of hot and cold

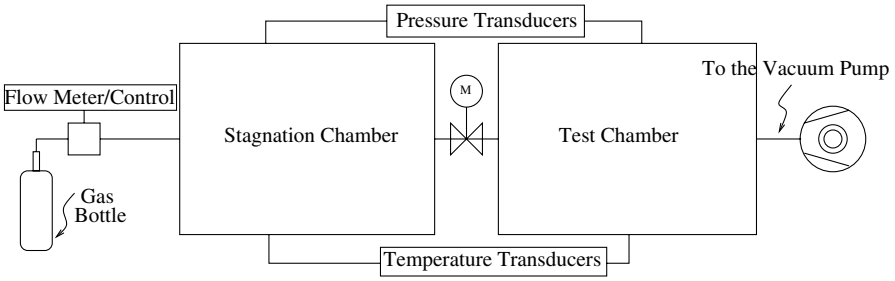

Fig. 1 Sketch of the experimental rig.

cathodes, and by thermocouples. The mass flow rates were controlled and measured by a Brooks 5850 instrument with a range of $(0.1–200) \times 10^{-8}$ kg/s and an accuracy of 2.4% on the minimum reading. Pressure measurements were obtained using a set of two absolute pressure transducers (MKS 672, with range of $10^{-2}–10^{2}$ Pa and an accuracy of 0.12% on the minimum reading) and with hot cathode ionization vacuum gauges (Pfeiffer IMR 112 and 125, with range of $10^{-8}–10^{2}$ Pa and an accuracy of 1% of minimum reading).

The Patterson probe, made by Hyperschalltechnologie (Göttingen), GmbH, is shown in Fig. 2. A rectangular orifice (with a width of $W = 1$ mm and a height of $H = 10$ mm) is open in a tube with an external diameter of 5 mm, a length of 55 mm, and a wall thickness of 0.25 mm. The axis of the tube is normal to the jet axis. The probe collects gas particles from the external stream and measures their number with a hot cathode head. All movements of the supporting sled are governed by step motors. The positions of the sounding slot can be changed by as little as 0.01 mm steps. The probe was modified so that the sounding tube and its slot can be rotated 360 deg around the longitudinal axis of the tube. The signals from the probe and all the other measurements are recorded and stored in a computer, which also performs the data reduction.

Figure 3 shows a sketch (not to scale) of the test chamber with the movable probe holder. The presence of the sounding tube does not affect the measurements in the free molecular regime, even when it is in close proximity to the jet source; this was proved, in particular, by the symmetry of the data.

III. Reduction of the Experimental Data

Let λ be the gas mean free path. The Knudsen number is $Kn_e = \lambda_e/D$, where $\lambda = 1/(\sqrt{2}\pi d^2 n)$ and d and n are the diameter and the number density of the molecules, respectively. The N_2 gas characteristics were taken from [17] and the subscript e signifies the values at the nozzle exit.

All the experiments were carried out with nitrogen, with stagnation chamber values of pressure, p_0^*, between 2.85 and 28.5 Pa

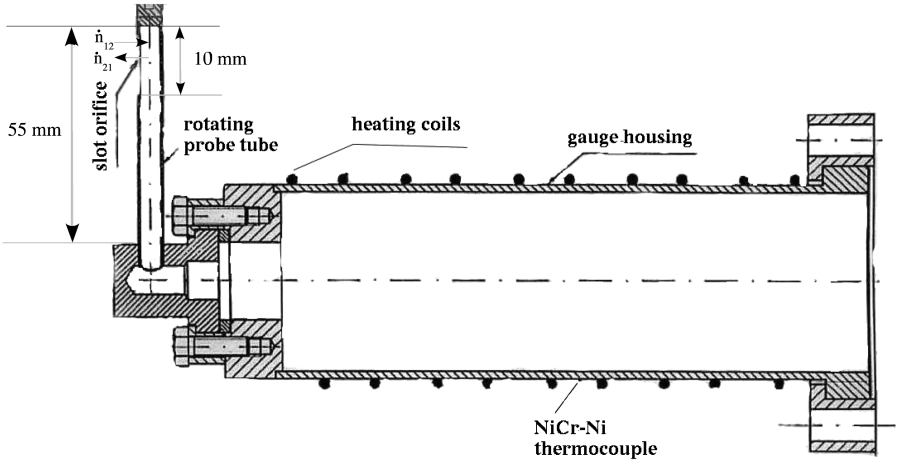

Fig. 2 Sketch of the Patterson probe (Hyperschalltechnologie GmbH).

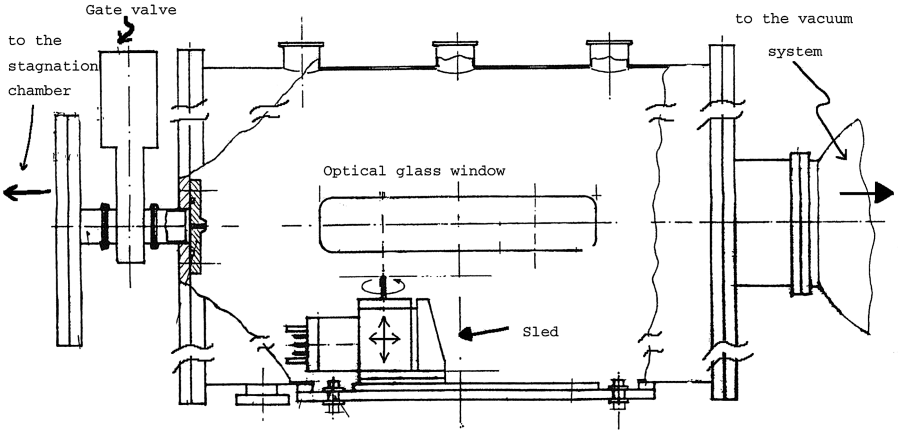

Fig. 3 Sketch of the test chamber with the Patterson probe holder.

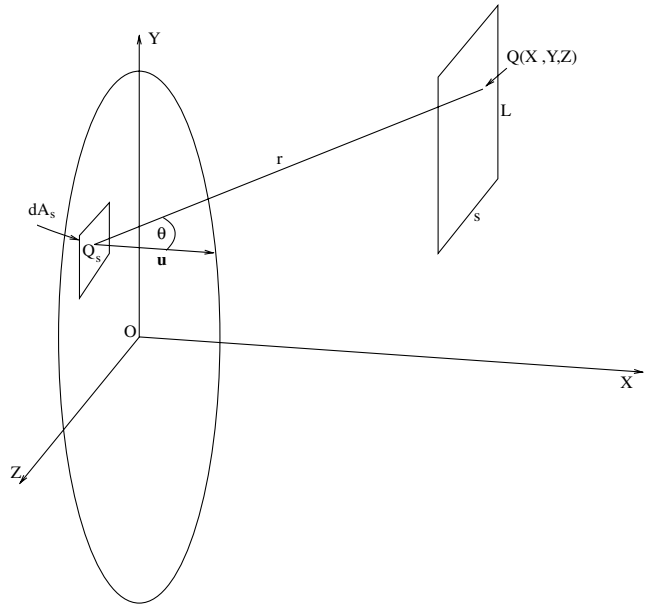

Fig. 4 Geometry of the flow region between the nozzle exit and the probe slot.

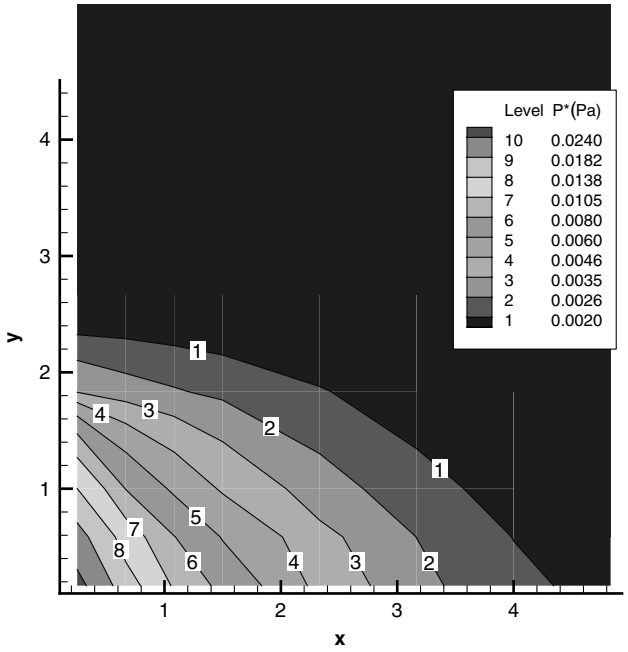

Fig. 5 Distribution of the measured pressure P^* (Pa) in the explored domain.

and a stagnation temperature equal to 300 K. Correspondingly, the Knudsen number at the jet inlet, Kn_i, ranges approximately between 0.36 and 0.036, and the values of Kn_e fall from well inside the range of free molecular to the transitional flow regime.

Figure 4 shows the geometry of the problem in which a system of orthogonal coordinates (X, Y, Z) has its origin in the center of the circular orifice and the X axis along the longitudinal axis of the jet. The axes (Y, Z) are parallel to the sides L and s of the slot, which has its center at $Z = 0$. All lengths here are normalized with respect to D.

Hot cathode readings were used to obtain the experimental values of $P^*(X, Y)$, the pressure distribution along the longitudinal axis of the jet, X, and in its normal direction, Y. These measurements were taken while the slot remained parallel to the orifice. At each X station, the transverse pressure profile was investigated. These runs were carried out in two directions, first with increasing and then with decreasing Y locations. The probe was initially located far from the jet to measure the ambient density and then moved to the opposite far side. If needed, the probe holder could also rotate a few degrees about a vertical axis to improve the alignment between the jet axis and the axis normal to the probe slot. Let α (0–180 deg) be the angular position of the sounding tube about its axis, where $\alpha = 0$ corresponds to the slot looking upstream. The measurements were carried out in three angular positions: $\alpha = 0$, 90, and 180 deg. Each run could last from several minutes to a few hours.

Figure 5 shows a map of the measured $P^*(X, Y)$ and a few iso-P^* lines in the explored domain for $p_0^* = 3.3$ Pa, $p_{\text{amb}}^* = 10^{-3}$ Pa, and $T_{\text{amb}} = 300$ K. Furthermore, and for the sake of clarity, Fig. 6 shows some representative Y profiles that were taken at selected positions along the X axis. Figure 7 shows some measured data along X for $Y = 0$. Figures 6 and 7 show the uncertainty bars for the adopted instrumentation chain. Note that after moving the sounding probe to a new location it was necessary to monitor the pressure signal for a rather long time until a steady state was reached, especially in the

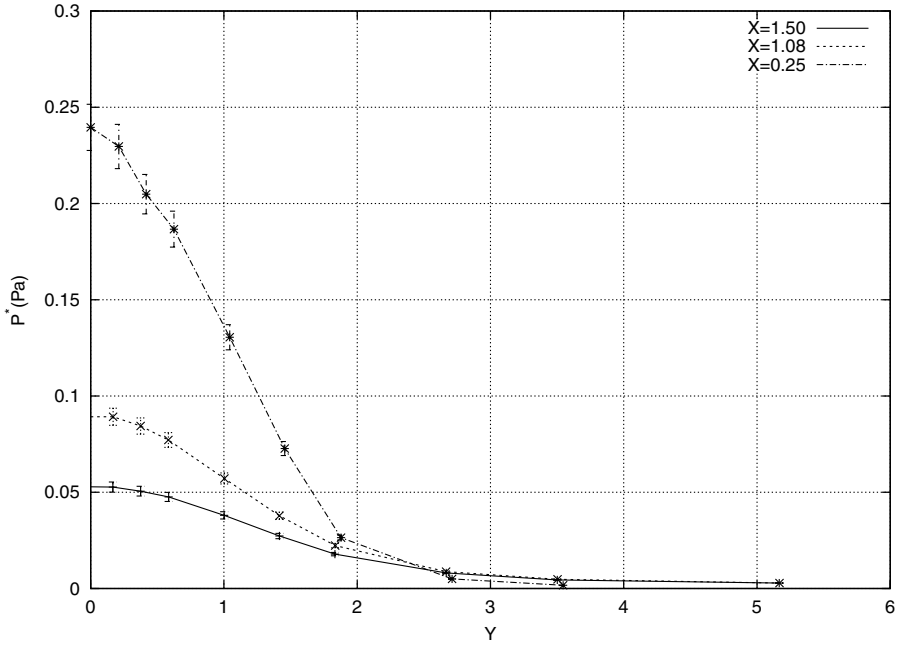

Fig. 6 Y profiles of measured pressures P^* (Pa) at selected X.

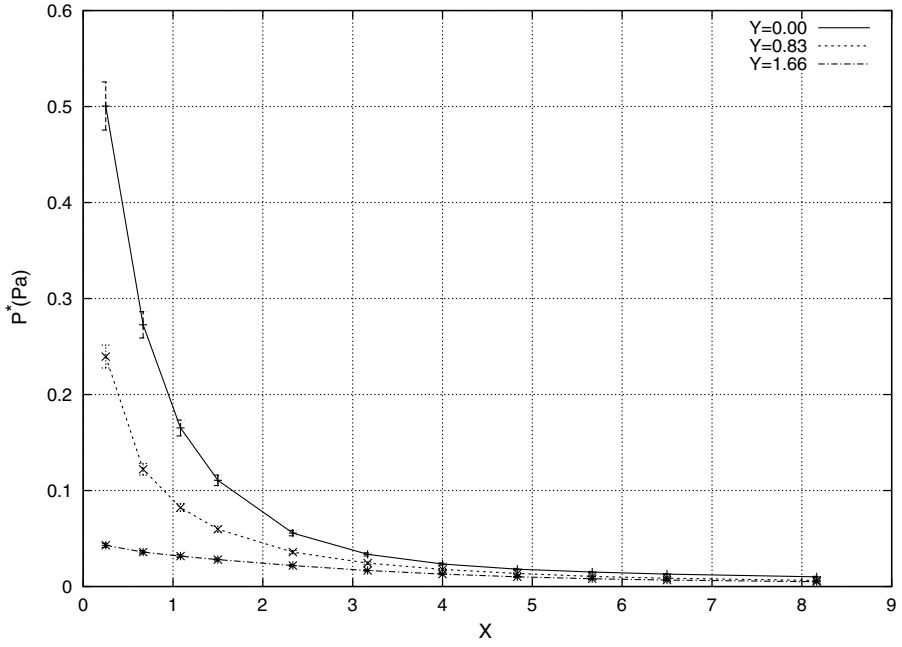

Fig. 7 ***X*** **profiles of measured pressures** ***P**** **(Pa) at selected** ***Y*****.**

more rarefied conditions. We use a capital P^* with reference to the mean pressure measured inside the probe. A lowercase p^* is used for local point values. For the data reduction, we assume that the number density n_e and the velocity u_e of the issuing flux is uniform over the nozzle exit and that the path traveled by each particle from the nozzle to the slot is the same. Then, the basic expressions reported by Koppenwallner [14] and Meyer [21] for the probe in a jet of free molecules can be used.

Referring to the geometry in Fig. 4, the molecules from an element dA_s of the jet round exit travel a distance r to reach a point Q of the probe slot. In our experimental apparatus, the density and the temperature in the stagnation chamber and in the test section were measured, whereas the mass flow rate $\dot{m}$ was imposed by the flow meter and controller. The flow across the cylindrical nozzle increases its initially low velocity as it proceeds to the exit while, simultaneously, the pressure is decreasing. From the round exit of the nozzle, a swarm of molecules of mean velocity $\langle u_e \rangle$ expands into the ambient region at $T_{\text{amb}} = 300$ K and $p^*_{\text{amb}} = 10^{-3}$ Pa. The mean velocity $\langle u_e \rangle$ can be calculated from the known mass flow rate. Furthermore, following the results presented by Koppenwallner et al. [1], Lilly et al. [4], and Sreekanth [22] for circular tubes, the final pressure at the nozzle exit $\langle p^*_e \rangle$ can be calculated as a function of the mass flow rate and of the ratio between the pressure values at the two ends of the nozzle.

Following Koppenwallner [14] and Meyer [21], a flux of free molecules with number density n_1 and temperature T_1 (pressure $p^*_1 = n_1 k T_1$) arrives at a point $Q(X, Y, Z)$ at the slot in the sounding tube. The molecular speed ratio is $S_1 = u/\sqrt{2\mathcal{R}T_1}$. The total number of molecules entering the cavity is computed by integration of the molecular flux over the aperture area $A = W \times H$. Inside the probe, a steady kinetic equilibrium (with number density n_2, temperature T_2, and pressure $p^*_2 = n_2 k T_2$) exists between the entering $\dot{n}_{12}$ and the outgoing $\dot{n}_{21}$ particles. The molecular speed ratio S is related to the Mach number by

$$S = \sqrt{\gamma/2}Ma$$

where γ the ratio of the specific heats.

The flux entering the probe is

$$\dot{n}_{12} = \frac{p^*_1}{m\sqrt{\pi}\sqrt{2\mathcal{R}T_1}}\chi(S_1 \cos\alpha)\tau_{12}$$

and the exit flux is

$$\dot{n}_{21} = \frac{p^*_2}{m\sqrt{\pi}\sqrt{2\mathcal{R}T_2}}\tau_{21}$$

where $\chi(S_1 \cos\alpha) = \exp(-(S_1 \cos\alpha)^2) + \sqrt{\pi}(S_1 \cos\alpha)[1 + erf(S_1 \cos\alpha)]$.

τ_{12} and τ_{21} are the transmission probabilities for free molecules entering and leaving the probe. In particular,

$$\tau_{12}(S_1, \alpha = 0, W/H) = 1 - 0.5(W/H)/(S_1\sqrt{\pi})$$

and

$$\tau_{12}(S_1, \alpha = 90, W/H) = 0.5(1 + \sqrt{\pi} ierfc(S_1 W/H))$$

where $ierfc$ is the first integral of the complementary error function [23]. For the adopted probe, $\tau_{21} = 0.89$, as specified by the manufacturer's data.

The ratio of the pressures p^*_2 and p^*_1 is given by

$$p^*_2/p^*_1 = \chi(S_1 \cos\alpha)\tau_{12}/\tau_{21}\sqrt{T_2/T_1}$$

If the pressure p^*_2 is measured at α equal to 0 and 90 deg, then the molecular speed ratio S_1 can be evaluated and, after measuring T_1 and T_2, the pressure p^*_1 is known.

Because of the relative dimensions of the measuring slot and the diameter of the longitudinal jet cross section, and because the transversal pressure distribution in the jet is not uniform, the measured P^* is actually the mean value of the pressure over the slot area p^*_m instead of the local p^*_1 value:

$$p^*_m(\bar{X}, Y) = 2/(Ls)\int_0^{s/2}\int_{Y-L/2}^{Y+L/2} p^*(y', z')\,\mathrm{d}y'\mathrm{d}z' \qquad (1)$$

where $L = H/D$ and $s = W/D$.

The calculations can be performed, at least in one significant case, by evaluating the dimensional values of p^*_m using Eq. (1). Figures 8 and 9 show the results of the transversal p^*_m distribution at two axial locations. In these results, the local values of p^* are calculated from the p^*_m values by putting the integral in Eq. (1) into its discretized Simpson form.

In the following section, we will compare the experimental p^*_m and p^* values, which have been calculated according to the aforementioned procedure, with the values calculated via the numerical–analytical method. Table 1 shows the measured mass

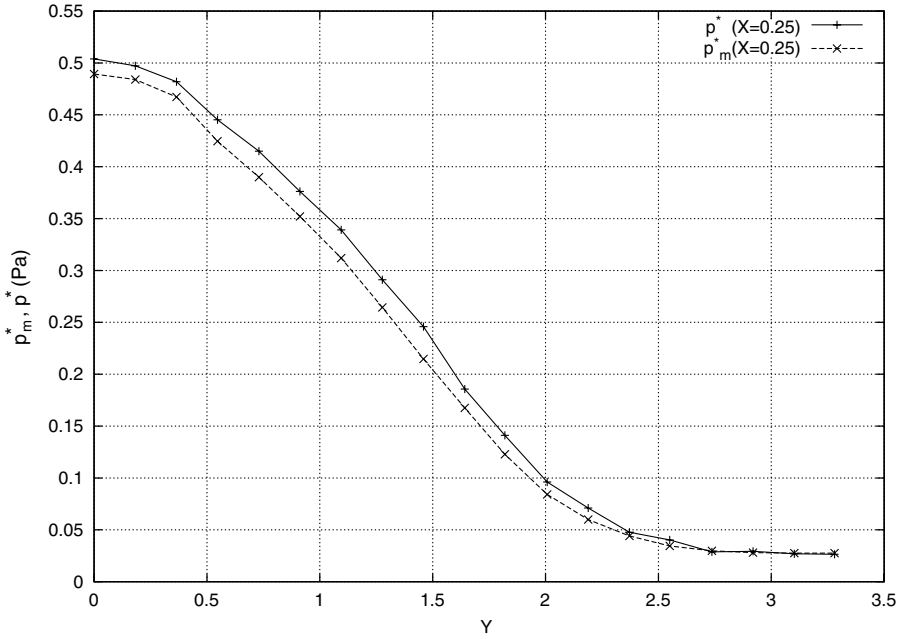

Fig. 8 Y profiles of measured pressures p_m^* (Pa) and the reduced local value p^* (Pa) at $X = 0.25$.

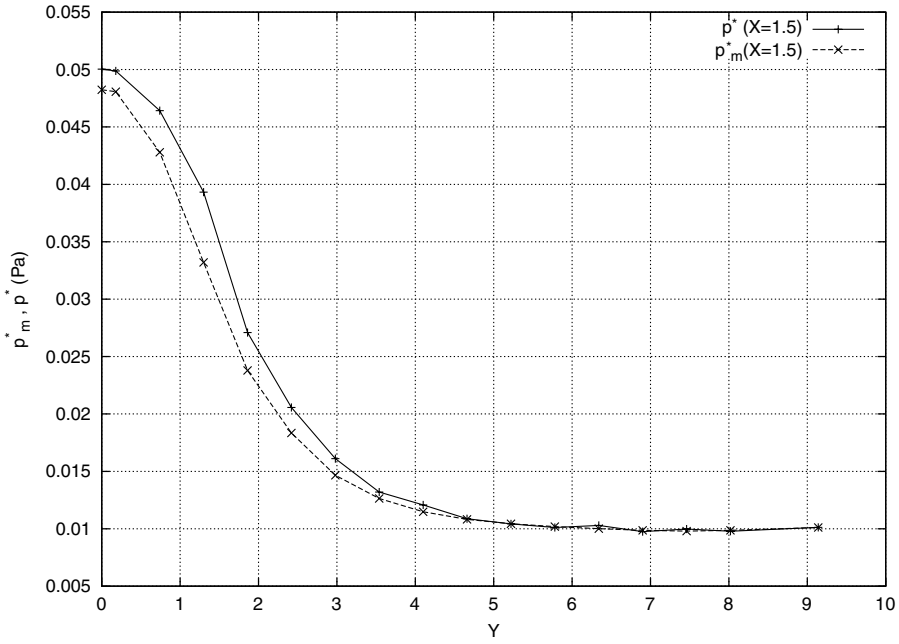

Fig. 9 Y profiles of measured pressures p_m^* (Pa) and the reduced local value p^* (Pa) at $X = 1.5$.

Table 1 Experimental readings of stagnation pressure p_0^*, ambient pressure p_{amb}^*, and mass flow rate $\dot{m}$

p_0^*, Pa	$p_{\text{amb}}^* \times 10^3$, Pa	$\dot{m} \times 10^8$, kg/s
1.5	2.5	1.9
2.7	4.5	3.8
3.3	5.5	4.8
3.9	6.5	5.8
4.4	8.0	6.7
5.0	9.0	7.7
5.5	10	8.6
5.9	12	9.6

flow rate $\dot{m}$ as a function of the pressure in the upstream stagnation chamber and of the pressure in the discharge chamber.

IV. Direct Simulation Monte Carlo Method Results

The direct simulation Monte Carlo code was used to simulate each of the experimental conditions. The results were used to evaluate the jet's initial thermofluid dynamic state after assigning the pressure in the upstream and downstream stagnation chambers. This DSMC procedure is similar to that reported by Sharipov [13] for a rarefied gas flow through an orifice in a thin wall and also that reported by Lilly et al. [4] for flow through tubes.

The adopted DSMC program was derived from the program described by Bird [17]. It is based on the numerical simulation of the

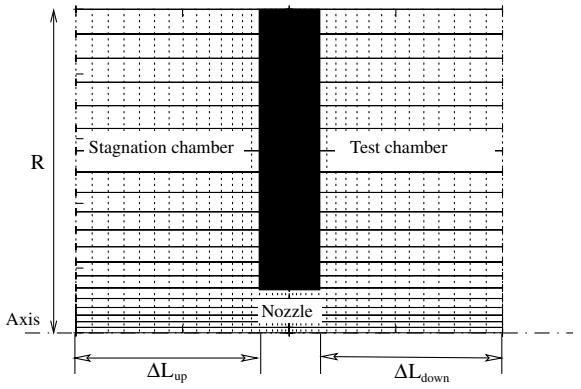

Fig. 10 Computational domain.

state (position and velocity) of a representative set of N_p molecules. The algorithm assumes a dilute gas and uses two different time scales, one for the collisions between molecules and the other for the motion of a molecule between collisions. Whereas the motion of the molecules is solved deterministically according to the laws of classical mechanics, the intermolecular collisions are handled as a stochastic process [4,13,17].

The fluid field encompasses the physical domain, composed of the stagnation chamber, the nozzle, and the test chamber. The ambient particles are modeled as normal particles entering the downstream boundaries. This simulation can be time consuming and can use a significant amount of computer memory to obtain a result with reasonable numerical accuracy, because it uses a large number of cells and representative particles. In our case, the computational domain (Fig. 10) was divided into a grid of nonuniform cells, with the smallest cells used at the nozzle where the flow gradients require more accuracy. The grid was generated using the hyperbolic tangent rule [24]. The computational time for the higher-density situation is an order of magnitude greater than it is for the lower-density situation. The total CPU time was about four weeks on an Intel Xeon 2.8 GHz processor for the case of $p_0^* = 34$ Pa.

The DSMC method requires accurate specification of the boundary conditions. We extended the domain both upstream and downstream of the nozzle to avoid regions of subsonic flow, so that the boundary conditions did not have to handle disturbances that travel upstream [4]. We performed several tests on domains of different dimensions. At the inflow boundaries, we assigned conditions of vanishing velocity and used stagnation values of the temperature and pressure. The interaction with the nozzle wall was handled using the diffusive reflection model [25]. Ambient values of the temperature and pressure were used at the borders of the test chamber.

The numerical accuracy of the DSMC method depends on the space discretization (cell size), the time discretization, the physical dimensions of the simulation domain, the number of representative molecules (N_p), and the number of samples used to evaluate the macroscopic parameters. An estimate of the numerical error was based on the norm [26]:

$$\varepsilon_\psi = \frac{1}{N}\sum_{k=1}^{N}\left|\left(\psi_k^i - \psi_k^{i-1}\right)/\psi_k^{i-1}\right|$$

where N is the number of cells, i is the numerical step, and ψ is either the macroscopic velocity u or the density ρ. The obtained values of ε are less than 10^{-5} for $\psi = \rho$ and less than 10^{-4} for $\psi = u$. We tested numbers for the representative molecules (N_p) ranging from 2.5×10^6 to 10×10^6; a value of 7.5×10^6 was chosen. Various sizes of the computational domain were tested. These dimensions (normalized by D) ranged from 5 to 20 for ΔL_{up} and ΔL_{down} and from 3 to 12 for R (Fig. 10). In all cases, the number of cells was greater than 10^4, and the time step Δt ranged from 0.005 to 0.001 μ_0/p_0^*, where μ_0 is the reference viscosity.

Figures 11 and 12 provide an example of the convergence of the numerical method, with results showing the influence of the domain size on the calculated pressure distribution. Figure 11 shows the axial pressure distribution, assuming different values of ΔL_{up} and ΔL_{down} at $R = 7$. Figure 12 gives the radial pressure distribution at $X = 0.3$ for ΔL_{up} and ΔL_{down} as both equal to 12. Note that the scale on the pressure axis is logarithmic, which makes it easier to appreciate small differences. Even on a logarithmic scale, the values of the radial pressure in Fig. 12 have negligible differences. Following these numerical experiments, all simulations were performed with $R = 7$ and $\Delta L_{\text{up}} = \Delta L_{\text{down}} = 12$.

Figure 13 shows the DSMC initial profiles of the dimensionless velocity S_e and the pressure p_e, which were subsequently used for the free molecular analysis of the jet. In particular, the pressure p^* and, later, p are normalized with respect to the mean pressure $\langle p_e^* \rangle$ at the nozzle exit.

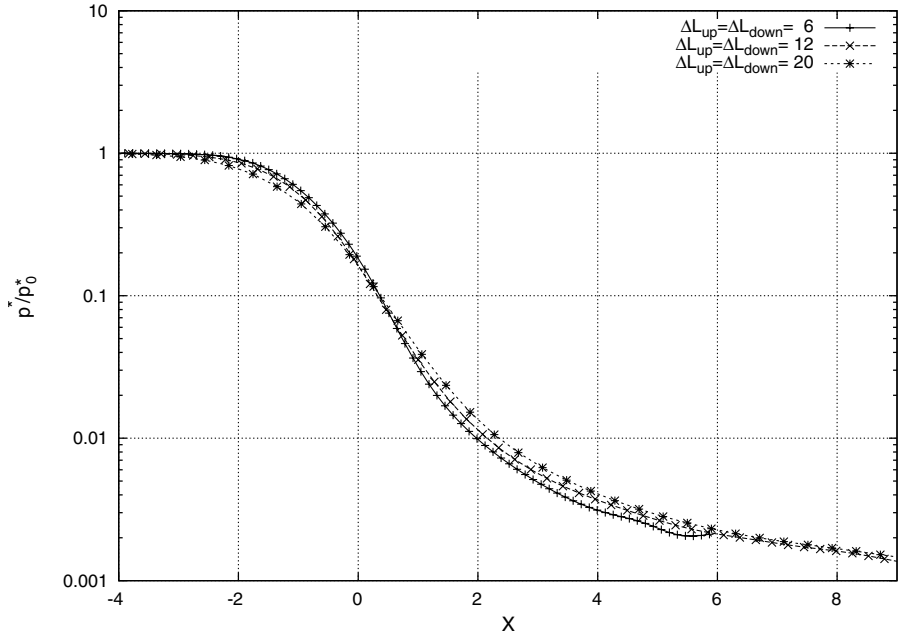

Fig. 11 Pressure distribution on the axis of the jet for $R = 7$ at different values of ΔL_{up} and ΔL_{down}.

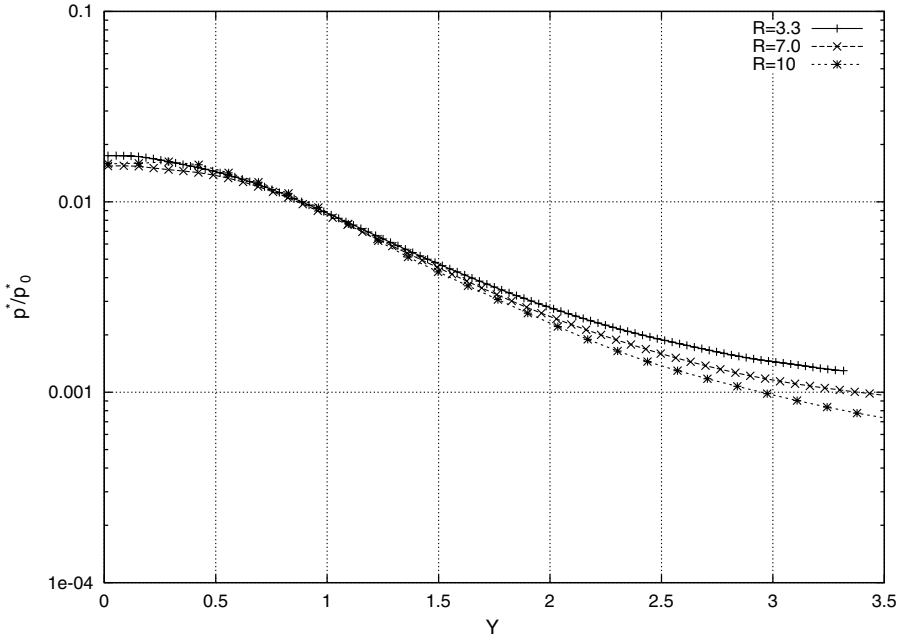

Fig. 12 Radial pressure distribution at different values of R; $X = 0.3$ and $\Delta L_{\text{up}} = \Delta L_{\text{down}} = 12$.

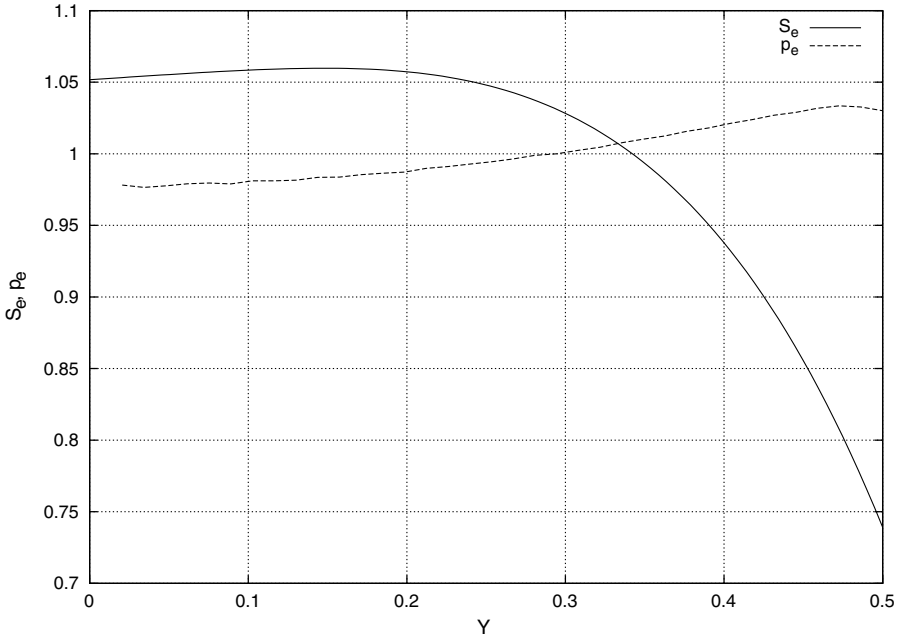

Fig. 13 DSMC initial profiles of the dimensionless velocity S_e and pressure p_e.

V. Free Molecular Solution

Consider pressure p at point $Q(X, Y, Z)$ (Fig. 4) for a flow of free molecules leaving the elemental surface dA_s and having a mean velocity along the X axis [27]:

$$p = \int_{A_s} p_e \pi^{-3/2} e^{-S_e^2} [(S_e/2)\cos\theta + (0.5 + S_e^2 \cos^2\theta) e^{(S_e^2 \cos^2\theta)} \sqrt{\pi}/2(1 + \text{erf}(S_e \cos\theta))]\, \text{d}\Omega \tag{2}$$

A_s is the area of the circular jet orifice, $\text{d}\Omega = (\mathbf{r} \times \mathbf{e}_X / r^3)\text{d}X_s\text{d}Y_s$ is the angle between $\text{d}A_s$ and Q, and θ is the angle between X and the flight direction of the molecules that contribute to the pressure at Q, that is, $\cos\theta = (\mathbf{r} \times \mathbf{e}_X / r)$ with $\mathbf{e}_X$ the unit vector along X.

The results of the DSMC simulations show that the dimensionless pressure distribution p_e (Fig. 13) is almost constant over the nozzle exit, with variations of less than 0.03. Therefore, based on Eq. (2), one can assume that p is a function of S_e only.

It is possible to evaluate the influence of a nonconstant radial velocity distribution at the nozzle exit using

$$p(S_e) = p(S_{e,0}) + \left[\frac{\text{d}p}{\text{d}S_e}\right]_{S_e = S_{e,0}} (S_e - S_{e,0}) + [\cdots]$$

where $\text{d}p/\text{d}S_e$ is the sensitivity of the p value at a given location with respect to the velocity profile at the nozzle exit. $S_{e,0}$ is the constant value of the thermal velocity for a constant discharge velocity. The sensitivity can be evaluated analytically from the following equation:

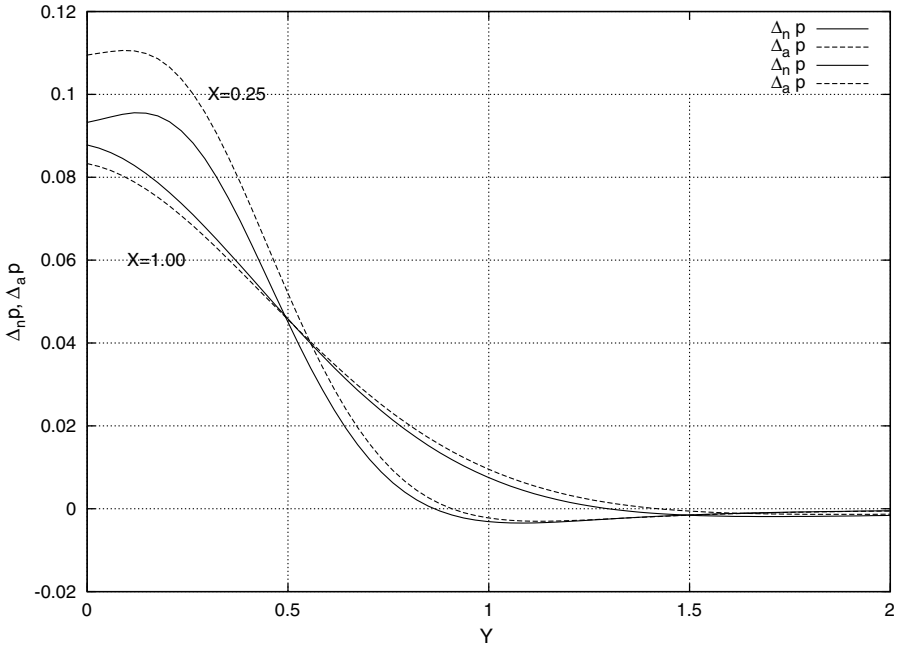

Fig. 14 Pressure differences $\Delta_n p$ and $\Delta_a p$ at two axial locations.

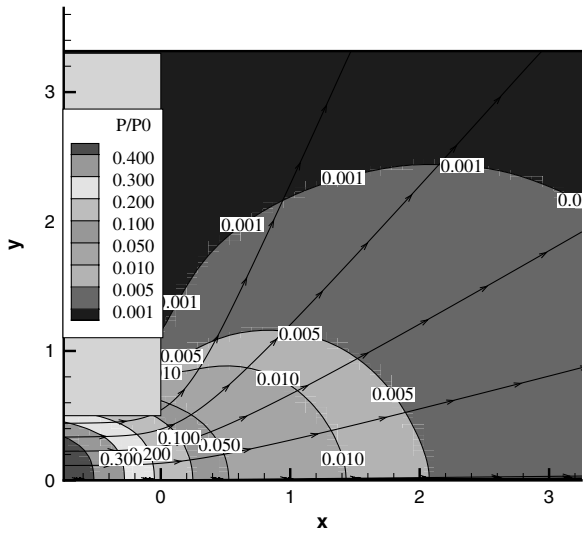

Fig. 15 p/p_0 and streamline distribution for $p_0^* = 0.34$ Pa.

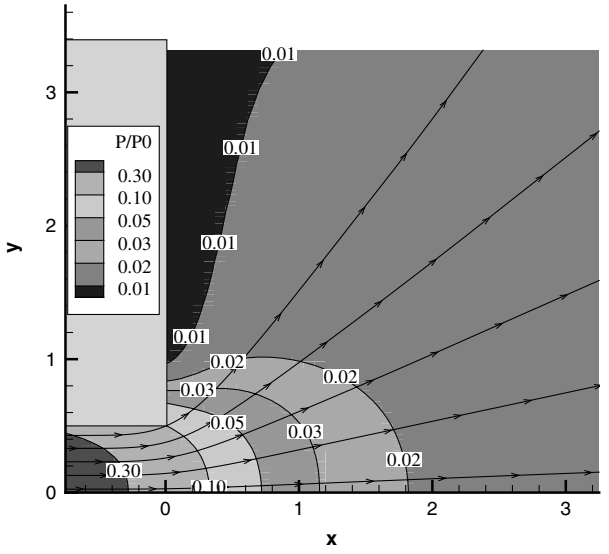

Fig. 17 p/p_0 and streamline distribution for $p_0^* = 34$ Pa.

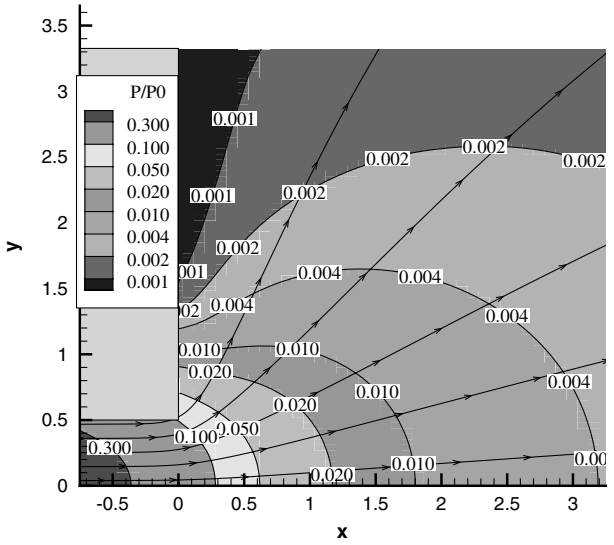

Fig. 16 p/p_0 and streamline distribution for $p_0^* = 3.4$ Pa.

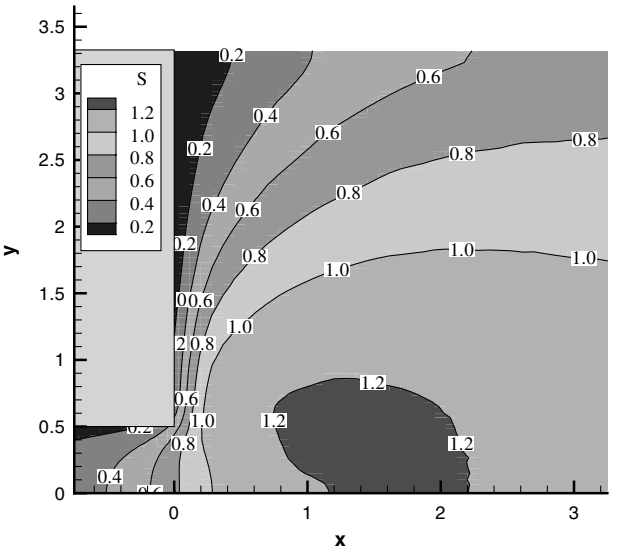

Fig. 18 S distribution for $p_0^* = 3.4$ Pa.

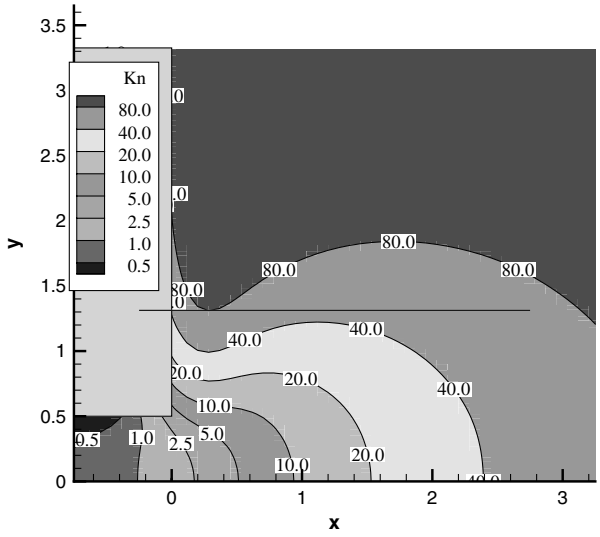

Fig. 19 ***Kn*** **distribution in the test chamber for** $p_0^* = 3.4$ **Pa.**

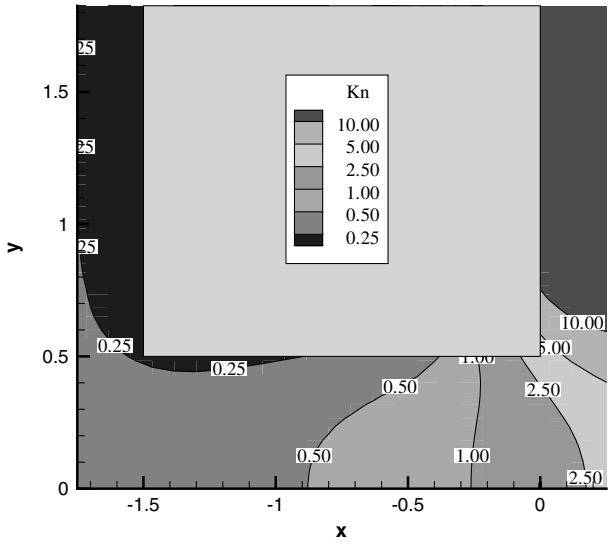

Fig. 20 ***Kn*** **distribution in the nozzle for** $p_0^* = 3.4$ **Pa.**

$$\frac{\mathrm{d}p}{\mathrm{d}S} = -2S_e p + \int_{A_s} \exp\left(-S_e^2\right)/\pi^{3/2}\left\{\cos\theta\left(1 + S_e^2\cos^2\theta\right)\right.$$
$$+ \exp(S^2\cos^2\theta)S\sqrt{\pi}[1 + \operatorname{erf}(S\cos\theta)]$$
$$\left.\times\,[0.5 + S^2(1 + \cos^2\theta)]\right\}\mathrm{d}\Omega \tag{3}$$

Figure 14 presents the radial values of two sets of data at two axial locations. The first set shows the difference $\Delta_n p$ between the pressure calculated from the initial velocity values provided by the DSMC method, $p_S = p(S_e)$, and the pressure $p_{S_0} = p(S_{e,0})$ calculated by taking a constant initial velocity distribution, $S_{e,0} = 1$. The mean value of p_S over the jet exit is also equal to 1.

The second set is the value of $\Delta_a p = [\mathrm{d}p/\mathrm{d}S_e]_{S_e = S_{e,0}}(S_e - S_{e,0})$, calculated via the sensitivity definition. We note that $\Delta_n p$ and $\Delta_a p$ converge to the same values far from the jet longitudinal axis in the radial direction; this effect is enhanced as X increases. The difference between $\Delta_n p$ and $\Delta_a p$ becomes negligible at 1-nozzle-diam distance from the nozzle exit. However, the influence of the initial velocity profile is dominant in the proximity of the jet orifice.

An examination of Fig. 14 shows that the sensitivity of the final results to the value of the gas velocity at the jet origin is not negligible. Consequently, after the DSMC code is validated with the experimental data, the numerically calculated gas state parameters at the nozzle exit can be taken as the initial condition for the free molecular calculations.

VI. Results

This section presents the results of the final analysis of the jet. Figures 15–17 show the pressure distributions, p^*, close to the nozzle exit for the following three values of the stagnation chamber p_0^*: (0.34, 3.4, 34) Pa. The corresponding Knudsen numbers at the exit, Kn_e, are 20, 2, and 0.2, respectively. These values fall in the range between the free molecular regime and transition flow. Also, the pressure gradients increase with denser gas conditions. The pressure p^* is normalized with p_0^*, and the axial and radial coordinates X and Y are normalized with the diameter D. The conditions in Fig. 16 duplicate a situation that was experimentally investigated. Figures 15–17 also show the mean trajectories of the particles as they leave the initial dense core of the jet and rapidly move to rectilinear paths.

Figures 18–20 duplicate the conditions of the experimental case, $p^* = 3.4$ Pa. Figure 18 shows the distribution of the molecular speed

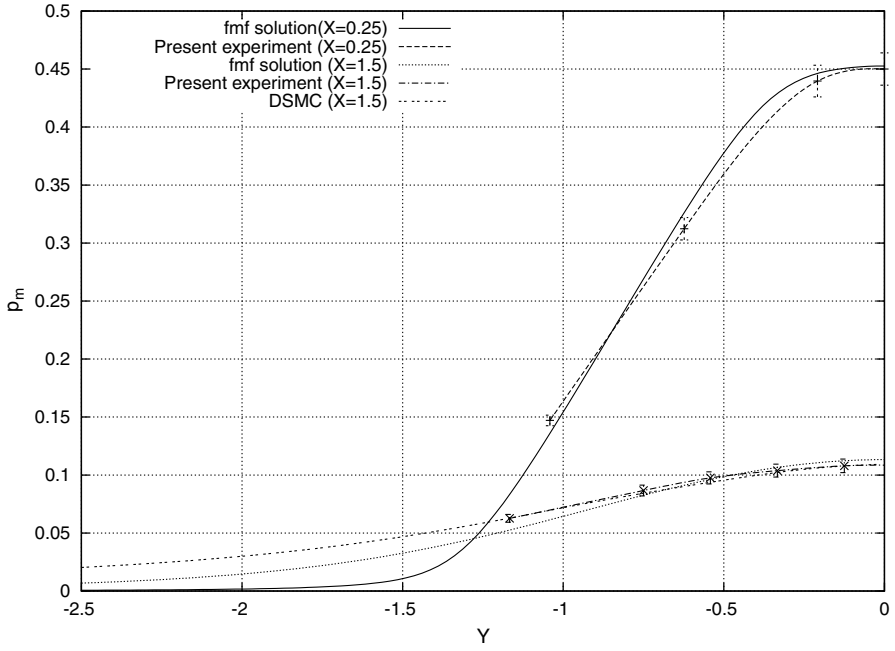

Fig. 21 ***Y*** **profiles of the calculated (DSMC and free molecular flow, or fmf) and reduced experimental pressure** p_m **at selected** X **(**$p_0^* = 3.4$ **Pa).**

ratio S. In this case, the gas leaves the nozzle at close to sonic conditions and accelerates to its maximum speed at a distance between 1 and 2 diameters from the exit. This effect is due to the limited dimension of the downstream ambient cavity and its temperature boundary condition. This appears in contrast with the results of Cai and Boyd [18], but that paper adopts an ad hoc turning off of the collisions between the molecules.

Continuum compressible flow phenomena such as a Mach disk or shock waves are not present. This can be more easily understood after considering Figs. 19 and 20, which show the local Kn values in the test chamber and in the nozzle. The flow actually reaches free molecular conditions by the nozzle exit and, clearly, a jet of free molecules interacts with the probe. Furthermore, Fig. 19 shows that the Kn value at the nozzle exit, Kn_e, is practically constant and equal to 2. The pressure and, consequently, the Knudsen number variations seen in Fig. 20 are in very close agreement with the data in Lilly et al. [4] for comparable conditions.

Figure 21 shows the results for a significant case. It provides a comparison of the reduced experimental p_m and the calculated pressure obtained by the free molecular flow solution and by the DSMC procedure. In particular, the comparisons shown at $p_0^* = 3.4$ Pa at $X = 1.5$, which matches the conditions of Fig. 9, are very good.

The reduced experimental data are also reported in Fig. 22, together with the analytically calculated free molecular flow values. Again, the comparison is quite satisfactory. The calculated values follow from the application of Eq. (2), with the initial S_e distribution as obtained via the DSMC method. These results show that the calculation may be limited to the stagnation chamber and to the nozzle, whereas the flow in the ambient region could be calculated instead by the free molecular flow analytical expressions using proper initial conditions.

Figure 23 shows the analytical free molecular description of the near jet mean pressure, taking the DSMC solution at the nozzle exit

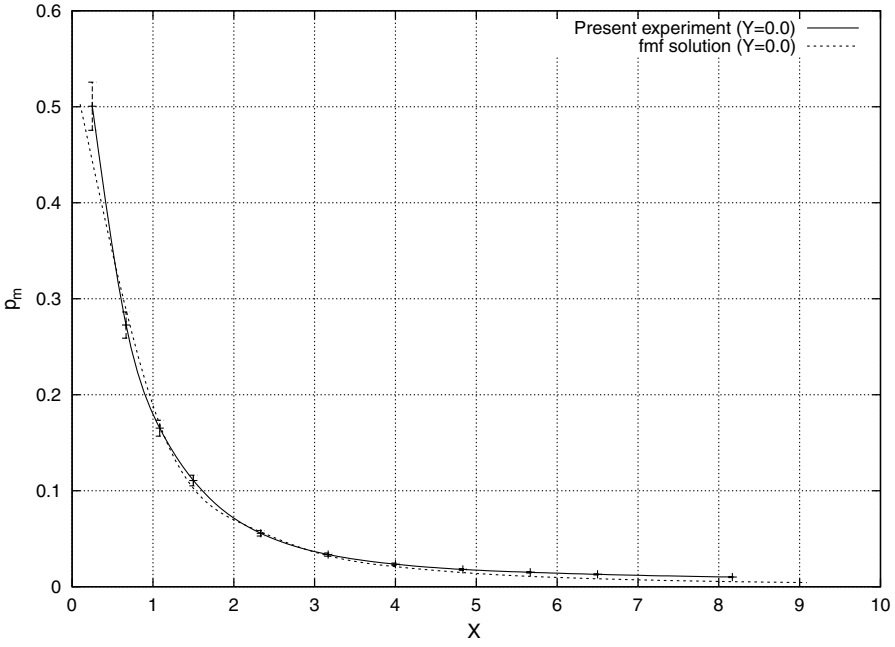

Fig. 22 X profiles of calculated (fmf) and reduced experimental pressures p_m at $Y = 0$ ($p_0^* = 3.4$ Pa).

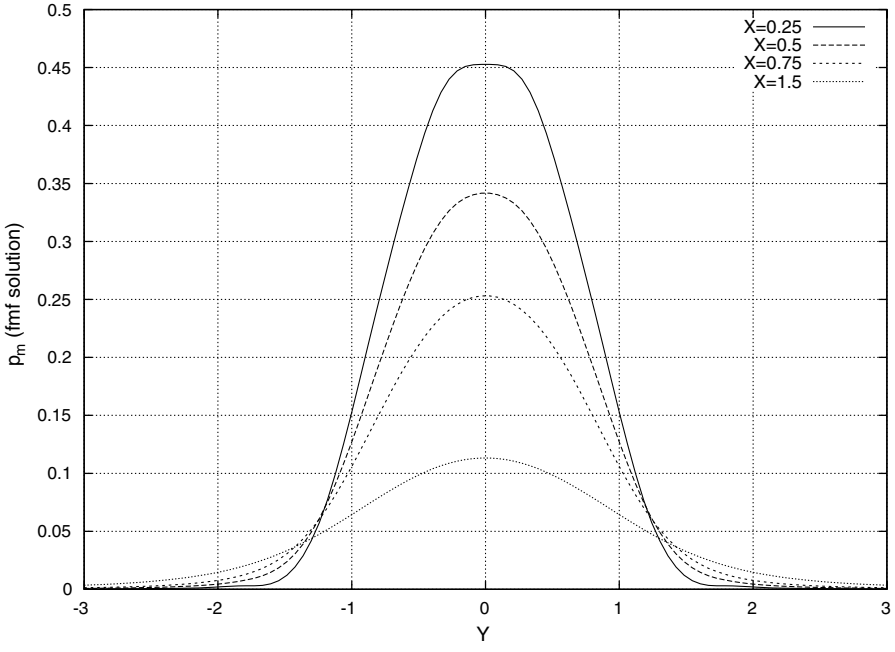

Fig. 23 Y profiles of the calculated (fmf) pressure p_m at selected X.

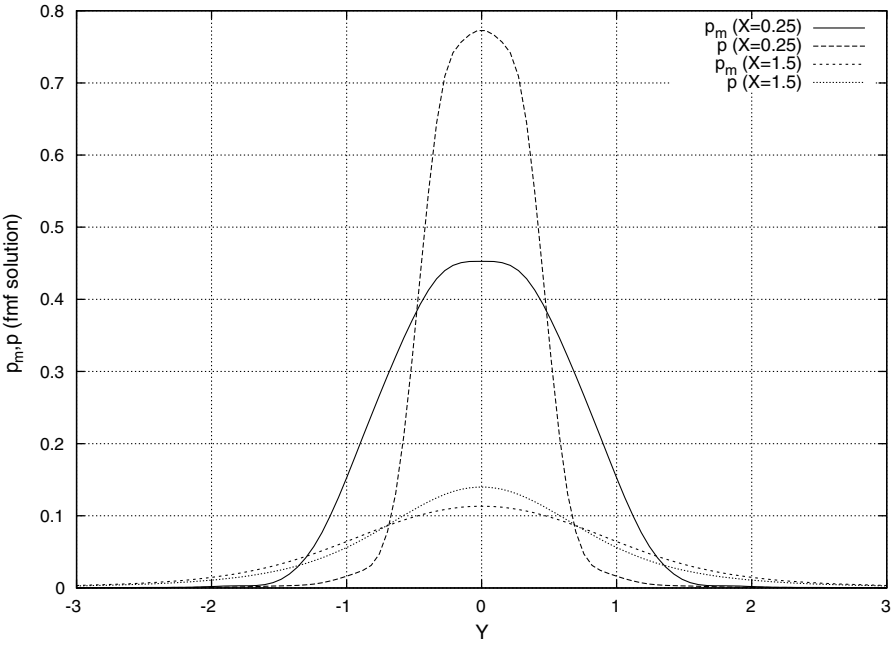

Fig. 24 *Y* profiles of the calculated (fmf) pressure p_m and p at selected X.

as the initial condition. The analytical Y profiles of p_m at various X are given for the same experimental conditions as those in Figs. 6 and 7. The radial profiles of p_m and p, also calculated by the free molecular flow expression and aided by the DSMC solution, are given in Fig. 24 at two values of X. Note that, close to the jet origin, the difference between p_m and p at the same Y distance can be as high as 100% of the p value.

Because of the averaging process of the probe sounding element, any errors in the local pressure measured at locations very close to the jet origin may lead to unacceptable errors in the results. However, the probe with its experimentally measured values provides an indispensable comparison for validating the DSMC simulations.

VII. Conclusions

The paper presented an analysis of the characteristics of a free molecule jet close to its origin. A numerical code for the DSMC simulations and an experimental apparatus were both demonstrated to be necessary for an accurate solution of the problem. We summarize this work with a few comments. With highly rarefied jets, a great deal of attention must be given to the full field when free molecules are present. In particular, the development of the flow from its stagnation state to the discharge ambient region should be taken into account when investigating the region close to the nozzle exit. Any a priori assumption concerning the initial characteristics of the jet should be carefully verified, and a sensitivity analysis should be performed. A Patterson impact probe can be an appropriate measurement device in terms of the cost-to-benefit ratio for validating the numerical–analytical results within the proper limits due to the averaging process of its slot dimensions.

Acknowledgment

This work has been partially supported by the Minister of Education, University and Research.

References

[1] Koppenwallner, G., Lips, T., and Dankert, C., "Discharge Coefficients and on Axis Flow Properties in Small Sonic Orifices at Low Reynolds Numbers," *Proceedings of the 25th Symposium on Rarefied Gas Dynamics*, Publishing House of the Siberian Branch of the Russian Academy, Novosibirsk, Russia, 2007, pp. 585–591.

[2] Rebrov, A. K., "Free Jets in Vacuum Technologies," *Journal of Vacuum Science and Technology*, Vol. 19, 2001, pp. 1679–1687. doi:10.1116/1.1382649

[3] Danilatos, G., "Direct Simulation Monte Carlo Study of Orifice Flow," *Proceedings of the 22nd Symposium on Rarefied Gas Dynamics*, Vol. 585, American Institute of Physics, Melville, NY, 2001, pp. 924–932.

[4] Lilly, T. C., Gimelshein, S. F., Ketsdever, A. D., and Markelov, G. N., "Measurements and Computations of Mass Flow and Momentum Flux Through Short Tubes in Rarefied Gases," *Physics of Fluids*, Vol. 18, Sept. 2006, pp. 093601-1–093601-11. doi:10.1063/1.2345681

[5] Naumann, K. W., "Analytical Method for Rapid Estimation of Plumes From Small Satellite Attitude Control Thrusters," *Proceedings of the 17th Symposium on Rarefied Gas Dynamics*, Wiley–VCH, Weinheim, Germany, 1990, pp. 971–978.

[6] Liepmann, H. W., "Gaskinetics and Gasdynamics of Orifice Flow," *Journal of Fluid Mechanics*, Vol. 10, No. 1, Feb. 1961, pp. 65–79. doi:10.1017/S002211206100007X

[7] Narashima, R., "Orifice Flow at High Knudsen Numbers," *Journal of Fluid Mechanics*, Vol. 10, No. 3, May 1961, pp. 371–384. doi:10.1017/S0022112061000986

[8] Woronowicz, M. S., and Rault, D. F. G., "On Plume Flowfield Analysis and Simulation Techniques," AIAA Paper 94-2048, June 1994.

[9] Ashkenas, H., and Sherman, F. S., "The Structure and Utilization of Supersonic Free Jets in Low Density Wind Tunnel," *Proceedings of the 5th Symposium on Rarefied Gas Dynamics*, Vol. 2, Academic Press, New York, 1966, pp. 84–105.

[10] Muntz, E. P., Hamel, B. B., and Maguire, B. L., "Some Characteristics of Exhaust Plume Rarefaction," *AIAA Journal*, Vol. 8, No. 9, Sept. 1970, pp. 1651–1658. doi:10.2514/3.49856

[11] Tartabini, P. V., Wilmoth, R. G., and Rault, D. E. F., "Direct Simulation Monte Carlo Calculations of a Jet Interaction Experiment," *Journal of Spacecraft and Rockets*, Vol. 32, 1995, pp. 75–84. doi:10.2514/3.26577

[12] Panda, J., and Seaholtz, R. G., "Density Measurements in Underexpanded Supersonic Jets Using Rayleigh Scattering," AIAA Paper 98-0281, 1998.

[13] Sharipov, F., "Numerical Simulation of Rarefied Gas Flow Through a Thin Orifice," *Journal of Fluid Mechanics*, Vol. 518, 2004, pp. 35–60. doi:10.1017/S0022112004000710

[14] Koppenwallner, G., "The Free Molecular Pressure Probe with Finite Length Slot Orifice," *Rarefied Gas Dynamics*, Vol. 1, Univ. of Tokyo Press, Tokyo, 1984, pp. 415–422.

[15] D'Ambrosio, D., de Socio, L. M., and Gaffuri, G., "Physical and Numerical Experiments on an Underexpanded Jet," *Meccanica*, Vol. 34, No. 4, Oct. 1999, pp. 267–280. doi:10.1023/A:1004799204306

[16] de Socio, L. M., Marino, L., "Gas Flow in a Permeable Medium," *Journal of Fluid Mechanics*, Vol. 557, 2006, pp. 119–133. doi:10.1017/S0022112006009621

[17] Bird, G. A., *Molecular Gas Dynamics and Direct Simulation of Gas Flows*, Oxford Univ. Press, Oxford, 1994.

[18] Cai, C., and Boyd, I. D., "Collisionless Gas Expanding into Vacuum," *Journal of Spacecraft and Rockets*, Vol. 44, No. 6, 2007, pp. 1326–1330.
doi:10.2514/1.32173

[19] Chue, S. H., "Pressure Probes for Fluid Measurements," *Progress in Aerospace Sciences*, Vol. 16, No. 2, 1975, pp. 147–223.
doi:10.1016/0376-0421(75)90014-7

[20] Rosenhauer, M., Plähn, K., and Hannemann, K., "Comparisons of Decoupled Hybrid Navier-Stokes-DSMC Calculations with Experiments in Plumes," *Proceedings of the 2-st Symposium on Rarefied Gas Dynamics*, Vol. 1, Cépaduès Éditions, Toulouse, France, 1999, pp. 671–678.

[21] Meyer, J. T., "Free Molecular Pressure Probe Measurements in the Continuum, Transitional and Free Molecular Regimes of a Free Jet," *Proceedings of the 17th Symposium on Rarefied Gas Dynamics*, Wiley–VCH, Weinheim, Germany, 1991, pp. 963–970.

[22] Sreekanth, A. K., "Transition flow through short circular tubes," *Physics of Fluids*, Vol. 8, No. 11, Nov. 1965, pp. 1051–1056.
doi:10.1063/1.1761142

[23] Kaye, J., "A Table of the First Eleven Repeated Integrals of the Error Function," *Journal of Mathematics and Physics*, Vol. 34, 1955, pp. 119–125.

[24] Orlandi, P., *Fluid Flow Phenomena: A Numerical Toolkit*, Kluwer, Dortrecht, The Netherlands, 2000.

[25] Cercignani, C., and Lampis, M., "Kinetic Model for Gas-Surface Interaction," *Transport Theory and Statistical Physics*, Vol. 4, 1971, pp. 1283–1289.

[26] de Socio, L. M., and Marino, L., "Numerical Experiments on the Gas Flow Between Eccentric Rotating Cylinders," *International Journal for Numerical Methods in Fluids*, Vol. 34, No. 3, 2000, pp. 229–240.
doi:10.1002/1097-0363(20001015)34:3<229::AID-FLD55>3.0.CO;2-5

[27] Nöller, H. G., "Approximate Calculation of Expansion of a Gas from Nozzles into High Vacuum," *Journal of Vacuum Science and Technology*, Vol. 3, No. 4, July 1966, pp. 202–207.
doi:10.1116/1.1492475